Interferometric Method for Direct Measurement of the Effective Mass in Two-Dimensional Systems

V. M. Muravev,[1,*] A. V. Shchepetilnikov,[1] K. R. Dzhikirba,[1] I. V. Kukushkin,[1] R. Schott,[2] E. Cheah,[2] W. Wegscheider,[2] and A. Shuvaev[3]

[1] *Institute of Solid State Physics, RAS, Chernogolovka 142432, Russia*
[2] *Solid State Physics Laboratory, ETH Zurich, Zurich CH-8093, Switzerland*
[3] *Institute of Solid State Physics, Vienna University of Technology, Vienna 1040, Austria*

(Received 10 September 2022; revised 27 October 2022; accepted 22 December 2022; published 14 February 2023)

We have developed a method of determining the effective mass of charge carriers in a two-dimensional electron system (2DES) based on the phase analysis of the radiation transmitted through the 2DES. This measurement technique is demonstrated in the experiments with a high-quality 2DES in InAs/AlSb and GaAs/(Al, Ga)As heterostructures. Furthermore, we find that the proposed approach gives compatible results with the cyclotron resonance spectroscopy method.

DOI: 10.1103/PhysRevApplied.19.024039

I. INTRODUCTION

The effective mass is a key parameter characterizing the band structure of semiconductors. The original and most common methods of measuring the mass in semiconductor two-dimensional systems is cyclotron resonance (CR) spectroscopy [1–3] and temperature-dependent Shubnikov–de Haas measurements [4–6]. The disadvantage of these techniques is that they cannot be applied to anisotropic systems. Moreover, CR experiments rely on rather strong external magnetic fields that can distort the Fermi surface and thereby influence the measured value of the mass. This effect is particularly significant for narrow-gap semiconductors [7]. An alternative approach is to use plasma excitation spectroscopy [8–17] or Fermi contour mapping using commensurability oscillations [18,19]. However, these methods require fabrication of a gridlike gate or microstructuring of the 2DES area.

In the present paper, we propose an interferometric method of measuring the effective mass of charge carriers in two-dimensional (2D) electronic systems. It is simple in implementation, noninvasive, and does not require any sample processing. The method relies on the phase analysis of the electromagnetic wave passing through a 2DES. Indeed, a recent experimental study has demonstrated that a two-dimensional electron layer can significantly change the phase of the electromagnetic wave traversing through it [20]. According to previous works [21–25], the 2DES impedance is well described by the Drude model as

$$Z_{\mathrm{2DES}}(\omega) = R + i\omega L_K, \qquad L_K = \frac{m^*}{n_s e^2}. \tag{1}$$

Here, n_s is the 2D electron density, m^* is the effective mass, and L_K is the kinetic inductance that arises from the collective motion of 2D electrons. Provided that $\omega L_K \gg R$, which is equivalent to $\omega\tau \gg 1$, the two-dimensional electron layer acts as 2D plasma. In that regime, the phase change of the radiation passing through the 2DES can be expressed as [26]

$$\Delta\phi = \arctan\frac{Z_0}{2\omega L_K}, \tag{2}$$

where $Z_0 = 377\,\Omega$ is the impedance of the vacuum. In order to eliminate the parasitic effects of the semiconductor substrate, $\Delta\phi$ measurements should be taken at Fabry-Pérot resonance frequencies $\omega_N = N\omega_d = Nc\pi/\sqrt{\varepsilon}d$ $(N = 1, 2, 3\ldots)$, where d denotes the substrate thickness. Thus, we can unambiguously determine the value of the electron mass along the direction of the electric field as follows:

$$m^* = \frac{Z_0}{2\omega_N}\frac{n_s e^2}{\tan\Delta\phi}. \tag{3}$$

II. METHODS AND SAMPLES

To determine the phase shift experimentally, we utilize the Mach-Zehnder interferometer, as illustrated in Fig. 1(a) [27]. A set of backward-wave oscillators (BWOs) is used as a source of radiation in the frequency range of $f = 50$–500 GHz. The diverging BWO beam is transformed into a quasiparallel beam by a collimating lens. Then, the grid polarizer (1) splits the electromagnetic radiation into the measurement and reference beams, indicated in Fig. 1(a) by yellow and pink colors, respectively. The beams in the measurement and reference arms of the

*muravev_vm@mail.ru

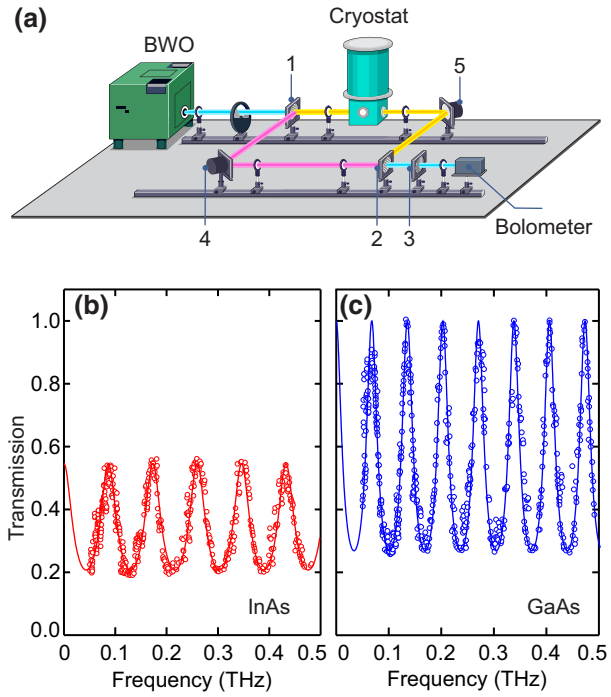

FIG. 1. (a) Schematic diagram of the Mach-Zehnder interferometer setup. (b) Transmission through the InAs/AlSb heterostructure measured at $B = 7$ T. The solid curve is the Fabry-Pérot function (4) calculated for the shunting dopant layer with the resistance per square $R_d = 530\ \Omega$ and the substrate thickness $d = 0.44$ mm at $\varepsilon_{\mathrm{GaSb}} = 15.7$. (c) Transmission through the GaAs/(Al, Ga)As heterostructure measured at $B = 7$ T. The solid curve is the Fabry-Pérot function (4) calculated for the substrate thickness $d = 0.62$ mm and $\varepsilon_{\mathrm{GaAs}} = 12.8$.

interferometer have orthogonal polarizations. The samples 1×1 cm^2 in size are cut out from a semiconductor wafer. The sample is placed inside an optical cryostat, at the center of a superconducting coil. The measurements are taken while maintaining the base sample temperature $T = 5$ K. The cryostat with the sample is placed in the measurement beam. The waves in the reference and measurement beams are added together at the grid (2) without any interference. In turn, the grid (3) lets pass a linear wave, allowing the corresponding components from the sample and reference beams to interfere. The interferometer is operated in such a way that, during the measurement, the position of the mobile mirror (4) in the reference arm is adjusted to maintain the balanced state of the interferometer, with zero signal on the detector. The interference signal modulated by the oscillating membrane mirror (5) is measured by the bolometer at the modulation frequency of 28 Hz. The displacement of the mirror (4) is then recalculated into the phase shift.

The proposed interferometric technique is tested on two wafers made of different semiconductor materials, both grown by molecular-beam epitaxy. The first wafer is a high-quality $Al_{0.33}Ga_{0.67}Sb/InAs/AlSb$ heterostructure grown on a GaSb substrate of thickness $d = 0.44$ mm, with a 20 nm InAs quantum well residing 25 nm below the crystal surface. The 2DES has an electron density of $n_{s1} = 7.44 \times 10^{11}$ cm^{-2} and a low-temperature mobility of 1.3×10^6 cm^2/V s. The second wafer is a standard industrial $GaAs/Al_{0.25}Ga_{0.75}As$ heterostructure grown on a GaAs substrate of thickness $d = 0.62$ mm. The structure hosts a two-dimensional electron system in a 20-nm-wide quantum well at a depth 220 nm below the crystal surface. In this case, the electron density in the quantum well is $n_{s2} = 1.30 \times 10^{12}$ cm^{-2}, with the low-temperature mobility reaching approximately 10^5 cm^2/V s. The electron densities of both samples are measured with very high accuracy based on the periodicity of the Shubnikov–de Haas oscillations.

III. RESULTS AND DISCUSSION

Figures 1(b) and 1(c) show the transmission spectra measured for the InAs/AlSb and GaAs/(Al, Ga)As heterostructure samples at a large magnetic field $B = 7$ T directed perpendicular to the sample surface. The applied magnetic field quenches the electron motion in the plane of the quantum well. Therefore, the resultant transmission in effect represents the behavior of the Fabry-Pérot function for a bare dielectric substrate, without 2DES. Notably, for the InAs/AlSb sample, the transmission at the Fabry-Pérot resonance does not reach the unity value ($|t_0|^2 = 0.55$), indicating the presence of a parallel conducting channel [28]. The existence of such a parasitic channel is independently confirmed by transport measurements. Indeed, it is quite common for semiconductor heterostructures similar to the sample under study. We expect this layer to be at the (Al, Ga)Sb/GaSb superlattice heterointerface located 270 nm below the sample surface. Its contribution to the sample impedance can be reduced to a simple shunt resistor R_d. As demonstrated by the solid curves in Fig. 1, the measured transmission dependencies are well approximated by the Fabry-Pérot function [29]:

$$T = \left| \frac{2}{\left(1 + \frac{Z_0}{R_d}\right) s_1 + s_2} \right|^2,$$
$$s_1 = \cos(kd) - \frac{i}{\sqrt{\varepsilon}} \sin(kd),$$
$$s_2 = \cos(kd) - i\sqrt{\varepsilon} \sin(kd), \tag{4}$$

where $k = \sqrt{\varepsilon}\omega/c$ is the radiation wave vector in the semiconductor substrate. For the GaSb substrate ($\varepsilon_{\mathrm{GaSb}} = 15.7$), the best fit of this function to the measurement data is achieved using the substrate thickness $d = 0.44$ mm and $R_d = 530\ \Omega$. Likewise, for the GaAs substrate ($\varepsilon_{\mathrm{GaAs}} = 12.8$), we obtain $d = 0.62$ mm, with R_d completely absent

(no shunting conductive layer). The thickness values determined from the Fabry-Pérot fits agree to good accuracy with those measured on the same samples directly with a mechanical gauge.

Having accurately determined the Fabry-Pérot resonance frequencies, we can proceed to find the phase. The simplest way to find the phase shift $\Delta\phi$ introduced by the 2DES at $B = 0$ T is to measure the wave phase ϕ as a function of the perpendicular magnetic field [Fig. 2(a)]. When the applied magnetic field grows strong, $\omega_c\tau = (eB/m^*)\tau \gg 1$ and $\omega_c \gg \omega$, it quenches the 2D plasma motion leading to the infinite 2DES impedance $Z_{2\mathrm{DES}}$. Indeed, the Drude conductivity in the presence of the magnetic field is

$$\frac{1}{Z_{2\mathrm{DES}}} = \sigma_{xx} = \frac{n_s e^2 \tau}{m^*} \frac{1 + i\omega\tau}{(1 + i\omega\tau)^2 + \omega_c^2 \tau^2}.$$

Clearly, at the infinite $Z_{2\mathrm{DES}}$, the two-dimensional layer makes no contribution to ϕ. Therefore, the phase shift can be determined as $\Delta\phi = \phi(5\ \mathrm{T}) - \phi(0\ \mathrm{T})$. As an example, Fig. 2(a) displays the phase as a function of the magnetic field at $f_{N=1} = 90$ GHz. The phase saturates at $B = 0.5$ T, demonstrating the full range of the phase shift of $\Delta\phi_{N=1} = 49^\circ$.

In Fig. 2(b), we show the dependence of $1/\tan\Delta\phi$ on the Fabry-Pérot resonance frequency f_N, measured for the InAs 2DES. The data (red dots) are well fitted by a linear curve (red line). Thus, the obtained linear dependence is consistent with Eq. (3). It should be noted that the presence of the parallel conductive layer slightly modifies this formula [26]:

$$m^* = \frac{Z_0}{2\omega_N} \frac{n_s e^2}{\tan\Delta\phi}\, t_0. \tag{5}$$

From the slope of the measured dependence, we unambiguously determine the effective mass of the electrons: $m^*_{\mathrm{InAs}} = (0.0352 \pm 0.0008)m_0$. This result agrees well with the values reported in the literature [7,30–32].

It should be noted that the proposed technique also works with samples that allow for in-situ density variation, say, with a metallic semitransparent gate. In this case, the tunability of the 2DES is accomplished by sweeping the gate voltage at $B = 0$ T [20]. The effect of the gate will be taken into account by the factor t_0 in Eq. (5), which can be determined directly from the amplitude of Fabry-Pérot resonances. However, it is more practical to quench the 2D plasma motion by the magnetic field because this approach does not need contacts with the 2DES and gate. In addition, thin semitransparent gates are very fragile and degrade quickly.

We test our method for the electric-field vector of the incident wave directed along different crystallographic

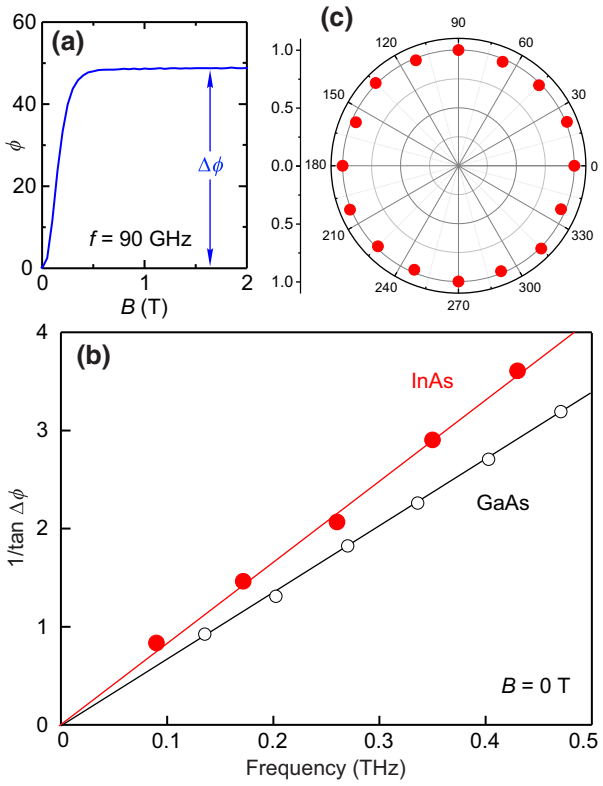

FIG. 2. (a) Phase of the electromagnetic wave passed through the 2DES ϕ plotted as a function of the magnetic field. (b) $1/\tan\Delta\phi$ versus the frequency f_N measured for the 2DESs in InAs/AlSb (red dots) and GaAs/(Al, Ga)As (black circles) heterostructures. (c) Mass ellipsoid in the InAs 2DES measured by rotating the electric field vector. The polar diagram is displayed in the measurement units of $m^*_{\mathrm{InAs}} = 0.0352m_0$.

directions. Then, the observed phase shift, $\Delta\phi$, is determined by the inertia of the electrons moving in the direction of the driving electric field. We conduct a series of experiments on the InAs 2DES sample. In each set of measurements, the electric field vector of the electromagnetic radiation at the interferometer input is pointed at a certain angle α with respect to the [110] crystallographic direction. As a result, we collect the data at $\alpha = 0^\circ, 22^\circ, 45^\circ, 67^\circ, 90^\circ, 112^\circ, 135^\circ, 157^\circ$, and 180°, obtaining the mass ellipsoid shown in Fig. 2(c). In this case, the polar plot corresponds to the measurement units of $m^*_{\mathrm{InAs}} = 0.0352m_0$. As expected, it represents a circle, reflecting the C_∞ symmetry of the Γ point in the Brillouin zone of InAs.

For the sake of comparison, Fig. 2(b) includes the plot of $1/\tan\Delta\phi$ versus f_N measured for the GaAs 2DES with the electron density $n_{s2} = 1.30 \times 10^{12}$ cm^{-2}. Using the same method, we find $m^*_{\mathrm{GaAs}} = (0.074 \pm 0.001)m_0$, which is in accordance with the CR spectroscopy studies of the same sample (see Supplemental Material [26]). Notably, this value is slightly larger than the band-edge mass in GaAs, $m^*_b = 0.0665m_0$. Presumably, the discrepancy is due to the nonparabolicity of the electron conduction band

occurring at such high 2D electron densities [33–35]. Indeed, for a GaAs quantum well with the energy of the ground electric level E_1, the effective mass becomes $m^*_{\mathrm{GaAs}} = m^*_b[1 + (2\alpha + \beta)E_1]$, where $\alpha = 0.642\ \mathrm{eV}^{-1}$ and $\beta = 0.697\ \mathrm{eV}^{-1}$ are the main nonparabolic and anisotropic terms, respectively, in the GaAs conduction band [34]. For a 20-nm quantum well with an electron density of $n_{s2} = 1.30 \times 10^{12}\ \mathrm{cm}^{-2}$, $E_1 \approx 50$ meV, one finds $m^*_{\mathrm{GaAs}} = 0.073m_0$, which agrees well with the experimental value.

In addition, we investigate the same InAs/AlSb heterostructure sample using the CR spectroscopy approach. Figure 3(a) shows the transmission through the sample versus the applied magnetic field, measured at $f = 90, 260$, and 430 GHz. A well-resolved CR is observed at both polarizations of the magnetic field. Notably, the measurement frequencies are selected to match the frequencies of the Fabry-Pérot modes, so that the substrate has no effect on the CR position [36,37]. The resultant CR magnetodispersion displayed in Fig. 3(b) is well described by the linear dependency $\omega_c = eB/m^*_c$ with $m^*_c = (0.0363 \pm 0.0007)m_0$. Thus, the values of the effective mass measured by the interferometric and CR spectroscopy methods are in good agreement.

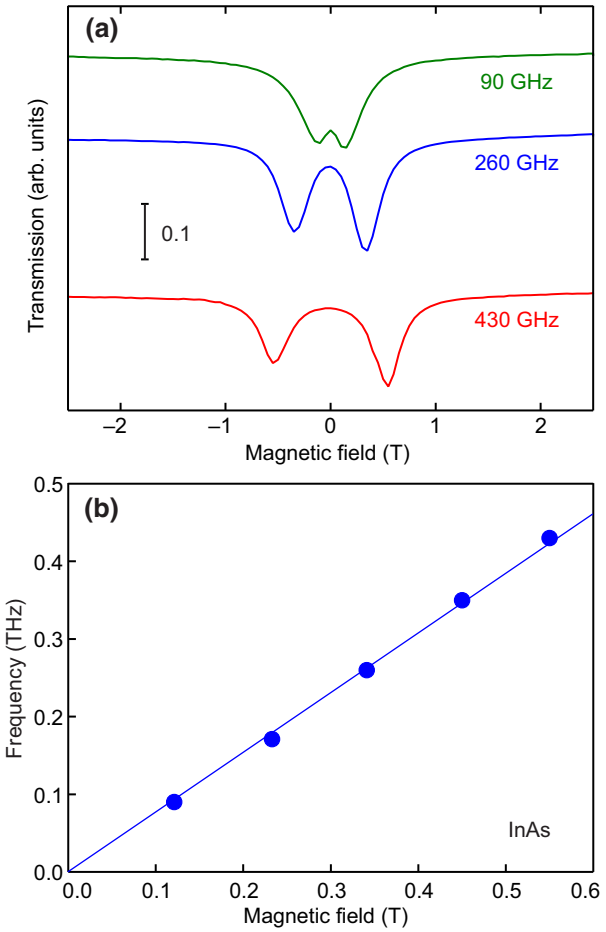

FIG. 3. (a) The magnetic-field sweep of the transmission recorded for the InAs 2DES at the radiation frequencies $f = 90$, 260, and 430 GHz. (b) Dependence of the CR resonant frequency on the applied magnetic field.

It is important to note that the basic Eq. (3) is applicable only if $\omega\tau \gg 1$, when the resistivity, R, of the 2DES impedance is small. In fact, detailed analysis [26] shows that taking into account the dissipation in a 2DES leads to an extra factor in (3) of the order of $(1 + 1/(\omega\tau)^2)$. In our case of a 2DES in the InAs/AlSb heterostructure, at $T = 5$ K and $f = 300$ GHz, $\omega\tau \approx 40$. Therefore, the effect of $\omega\tau$ in our experiments is negligible.

In conclusion, we develop an interferometric method for the direct measurement of the effective mass in two-dimensional systems. It is noninvasive and does not require any sample processing. The given experimental approach is validated by way of measuring a high-quality 2DES in InAs/AlSb and GaAs/(Al, Ga)As nanostructures. The resultant values of the effective mass $m^*_{\mathrm{InAs}} = (0.0352 \pm 0.0008)m_0$ at $n_{s1} = 7.44 \times 10^{11}\ \mathrm{cm}^{-2}$ and $m^*_{\mathrm{GaAs}} = (0.074 \pm 0.001)m_0$ at $n_{s2} = 1.30 \times 10^{12}\ \mathrm{cm}^{-2}$ are in good agreement with previous research. The proposed technique has prospects in exploring the energy spectrum in various solid-state systems.

ACKNOWLEDGMENTS

The authors gratefully acknowledge financial support from the Russian Science Foundation (Grant No. 18-72-10072 for the theory and idea and Grant No. 19-72-30003 for the experiment). The data supporting the findings reported in the present study are available from the corresponding authors upon request.

[1] G. Dresselhaus, A. F. Kip, and C. Kittel, Cyclotron resonance of electrons and holes in silicon and germanium crystals, Phys. Rev. **98**, 368 (1955).
[2] G. Abstreiter, P. Kneschaurek, J. P. Kotthaus, and J. F. Koch, Cyclotron Resonance of Electrons in an Inversion Layer on Si, Phys. Rev. Lett. **32**, 104 (1974).
[3] S. James Allen, D. C. Tsui, and J. V. Dalton, Far-Infrared Cyclotron Resonance in the Inversion Layer of Silicon, Phys. Rev. Lett. **32**, 107 (1974).
[4] I. M. Lifshitz and A. M. Kosevich, Theory of magnetic susceptibility in metals at low temperature, Sov. Phys. JETP **29**, 730 (1956).
[5] J. L. Smith and P. J. Stiles, Electron-Electron Interactions Continuously Variable in the Range $2.1 > r_s > 0.9$, Phys. Rev. Lett. **29**, 102 (1972).
[6] V. M. Pudalov, M. E. Gershenson, H. Kojima, N. Butch, E. M. Dizhur, G. Brunthaler, A. Prinz, and G. Bauer, Low-Density Spin Susceptibility and Effective Mass of Mobile Electrons in Si Inversion Layers, Phys. Rev. Lett. **88**, 196404 (2002).
[7] M. J. Yang, P. J. Lin-Chung, B. V. Shanabrook, J. R. Waterman, R. J. Wagner, and W. J. Moore, Enhancement

of cyclotron mass in semiconductor quantum wells, Phys. Rev. B **47**, 1691 (1993).

[8] C. C. Grimes and G. Adams, Observation of Two-Dimensional Plasmons and Electron-Ripplon Scattering in a Sheet of Electrons on Liquid Helium, Phys. Rev. Lett. **36**, 145 (1976).

[9] S. J. Allen, D. C. Tsui, and R. A. Logan, Observation of the Two-Dimensional Plasmon in Silicon Inversion Layers, Phys. Rev. Lett. **38**, 980 (1977).

[10] T. N. Theis, J. P. Kotthaus, and P. J. Stiles, Two-dimensional magnetoplasmon in the silicon inversion layer, Solid State Commun. **24**, 273 (1977).

[11] D. Heitmann, Two-dimensional plasmons in homogeneous and laterally microstructured space charge layers, Surf. Sci. **170**, 332 (1986).

[12] L. Ju, B. Geng, J. Horng, C. Girit, M. Martin, Z. Hao, H. A. Bechtel, X. Liang, A. Zettl, and Y. R. Shen, Graphene plasmonics for tunable terahertz metamaterials, Nat. Nanotechnol. **6 [10]**, 630 (2011).

[13] J. Chen, M. Badioli, P. Alonso-Gonzalez, S. Thongrattanasiri, F. Huth, J. Osmond, M. Spasenovic, A. Centeno, A. Pesquera, P. Godignon, A. Zurutuza Elorza, N. Camara, F. Abajo, R. Hillenbrand, and Frank H. L. Koppens, Optical nano-imaging of gate-tunable graphene plasmons, Nature **487**, 77 (2012).

[14] Z. Fei, A. S. Rodin, G. O. Andreev, W. Bao, A. S. McLeod, M. Wagner, L. M. Zhang, Z. Zhao, M. Thiemens, G. Dominguez, M. M. Fogler, A. H. Castro Neto, C. N. Lau, F. Keilmann, and D. N. Basov, Gate-tuning of graphene plasmons revealed by infrared nano-imaging, Nature **487**, 82 (2012).

[15] Qi Zhang, T. Arikawa, E. Kato, J. L. Reno, W. Pan, J. D. Watson, M. J. Manfra, M. A. Zudov, M. Tokman, M. Erukhimova, A. Belyanin, and J. Kono, Superradiant Decay of Cyclotron Resonance of Two-Dimensional Electron Gases, Phys. Rev. Lett. **113**, 047601 (2014).

[16] T. Herrmann, I. A. Dmitriev, D. A. Kozlov, M. Schneider, B. Jentzsch, Z. D. Kvon, P. Olbrich, V. V. Bel'kov, A. Bayer, D. Schuh, D. Bougeard, T. Kuczmik, M. Oltscher, D. Weiss, and S. D. Ganichev, Analog of microwave-induced resistance oscillations induced in GaAs heterostructures by terahertz radiation, Phys. Rev. B **94**, 081301(R) (2016).

[17] Jerzy Lusakowski, Plasmon–terahertz photon interaction in high-electron-mobility heterostructures, Semicond. Sci. Technol. **32**, 013004 (2016).

[18] D. Kamburov, Yang Liu, M. Shayegan, L. N. Pfeiffer, K. W. West, and K. W. Baldwin, Composite Fermions with Tunable Fermi Contour Anisotropy, Phys. Rev. Lett. **110**, 206801 (2013).

[19] M. A. Mueed, D. Kamburov, Yang Liu, M. Shayegan, L. N. Pfeiffer, K. W. West, K. W. Baldwin, and R. Winkler, Composite Fermions with a Warped Fermi Contour, Phys. Rev. Lett. **114**, 176805 (2015).

[20] V. M. Muravev, A. Shuvaev, A. S. Astrakhantseva, P. A. Gusikhin, I. V. Kukushkin, and A. Pimenov, Tunable terahertz phase shifter based on GaAs semiconductor technology, Appl. Phys. Lett. **121**, 051101 (2022).

[21] P. J. Burke, I. B. Spielman, J. P. Eisenstein, L. N. Pfeiffer, and K. W. West, High frequency conductivity of the high-mobility two-dimensional electron gas, Appl. Phys. Lett. **76**, 745 (2000).

[22] G. C. Dyer, G. R. Aizin, S. J. Allen, A. D. Grine, D. Bethke, J. L. Reno, and E. A. Shaner, Induced transparency by coupling of Tamm and defect states in tunable terahertz plasmonic crystals, Nat. Photon. **7**, 925 (2013).

[23] H. Yoon, K. Yeung, P. Kim, and D. Ham, Plasmonics with two-dimensional conductors, Philos. Trans. R. Soc. A **372**, 20130104 (2014).

[24] H. Yoon, C. Forsythe, L. Wang, N. Tombros, K. Watanabe, T. Taniguchi, J. Hone, P. Kim, and D. Ham, Measurement of collective dynamical mass of Dirac fermions in graphene, Nat. Nanotechnol. **9**, 594 (2014).

[25] V. M. Muravev, N. D. Semenov, I. V. Andreev, P. A. Gusikhin, and I. V. Kukushkin, A tunable plasmonic resonator using kinetic 2D inductance and patch capacitance, Appl. Phys. Lett. **117**, 151103 (2020).

[26] See Supplemental Material http://link.aps.org/supplemental/10.1103/PhysRevApplied.19.024039 for the derivation of transmittance in cases of the 2DES placed in the vacuum and the 2DES shunted by the parallel conductive layer. Also, the Supplementary Material gives CR spectroscopy data for the GaAs/(Al, Ga)As heterostructure.

[27] G. Kozlov and A. Volkov, *Millimeter and Submillimeter Wave Spectroscopy of Solids*, edited by G. Grüner (Springer-Verlag Berlin-Heidelberg, 1998), Vol. 74.

[28] P. A. Gusikhin, V. M. Muravev, K. R. Dzhikirba, A. Shuvaev, A. Pimenov, and I. V. Kukushkin, Effect of a conductive layer on Fabry-Pérot resonances, Phys. Rev. B **104**, 115408 (2021).

[29] Martin Dressel and George Grüner, *Electrodynamics of Solids: Optical Properties of Electrons in Matter* (Cambridge University Press, Cambridge, 2003), 1st ed.

[30] J. Scriba, A. Wixforth, J. P. Kotthaus, C. R. Bolognesi, C. Nguyen, G. Tuttle, J. H. English, and H. Kroemer, The effect of Landau quantization on cyclotron resonance in a non-parabolic quantum wells, Semicond. Sci. Technol. **8**, S133 (1993).

[31] J. Nehls, T. Schmidt, U. Merkt, D. Heitmann, A. G. Norman, and R. A. Stradling, Direct manifestation of the Fermi pressure in a two-dimensional electron system, Phys. Rev. B **54**, 7651 (1996).

[32] A. Ikonnikov, S. Krishtopenko, V. Gavrilenko, Y. Sadofyev, Y. Vasilyev, M. Orlita, and W. Knap, Splitting of cyclotron resonance line in InAs/AlSb QW heterostructures in high magnetic fields: effects of electron-electron and electron-phonon interaction, J. Low Temp. Phys. **159**, 197 (2010).

[33] Francisco A. P. Osório, M. H. Degani, and O. Hipólito, Cyclotron mass of electrons in GaAs-$Ga_1 - xAl_xAs$ quantum wells, Phys. Rev. B **38**, 8477 (1988).

[34] U. Ekenberg, Nonparabolicity effects in a quantum well: sublevel shift, parallel mass, and Landau levels, Phys. Rev. B **40**, 7714 (1989).

[35] S. Huant, A. Mandray, and B. Etienne, Nonparabolicity effects on cyclotron mass in GaAs quantum wells, Phys. Rev. B **46**, 2613 (1992).

[36] P. A. Gusikhin, V. M. Muravev, and I. V. Kukushkin, Superluminal electromagnetic two-dimensional plasma waves, Phys. Rev. B **102**, 121404(R) (2020).

[37] A. Shuvaev, V. M. Muravev, P. A. Gusikhin, J. Gospodarič, A. Pimenov, and I. V. Kukushkin, Discovery of Two-Dimensional Electromagnetic Plasma Waves, Phys. Rev. Lett. **126**, 136801 (2021).